



HAL
open science

Experimental Periodic Korteweg-de Vries Solitons along a Torus of Fluid

Filip Novkoski, Chi-Tuong Pham, Eric Falcon

► **To cite this version:**

Filip Novkoski, Chi-Tuong Pham, Eric Falcon. Experimental Periodic Korteweg-de Vries Solitons along a Torus of Fluid. 2022. hal-03649664v1

HAL Id: hal-03649664

<https://hal.science/hal-03649664v1>

Preprint submitted on 22 Apr 2022 (v1), last revised 14 Jun 2022 (v2)

HAL is a multi-disciplinary open access archive for the deposit and dissemination of scientific research documents, whether they are published or not. The documents may come from teaching and research institutions in France or abroad, or from public or private research centers.

L'archive ouverte pluridisciplinaire **HAL**, est destinée au dépôt et à la diffusion de documents scientifiques de niveau recherche, publiés ou non, émanant des établissements d'enseignement et de recherche français ou étrangers, des laboratoires publics ou privés.

Experimental Periodic Korteweg–de Vries Solitons along a Torus of Fluid

Filip Novkoski,^{1,*} Chi-Tuong Pham,^{2,†} and Eric Falcon^{1,‡}

¹Université Paris Cité, MSC, UMR 7057 CNRS, F-75013 Paris, France

²Université Paris-Saclay, LISN, UMR 9015 CNRS, F-91405 Orsay, France

(Dated: March 22, 2022)

We report on the experimental observation of solitons propagating along a torus of fluid. We show that such a periodic system leads to significant differences compared to the classical plane geometry. In particular, we highlight the observation of subsonic elevation solitons, and a nonlinear dependence of the soliton velocity on its amplitude. The soliton profile, velocity, collision, and dissipation are characterized using high resolution space–time measurements. By imposing *periodic boundary conditions* onto Korteweg–de Vries (KdV) equation, we recover these observations. A nonlinear spectral analysis of solitons (periodic inverse scattering transform) is also implemented and experimentally validated in this periodic geometry. Our work thus reveals the importance of periodicity for studying solitons and could be applied to other fields involving periodic systems governed by a KdV equation.

Introduction.— Since their first observation on the surface of water [1], solitons have been widely studied in various domains (including acoustics [2], plasmas [3], carbon nanotubes [4], Bose–Einstein condensates [5, 6], or blood vessels of living organisms [7]). Korteweg and de Vries (KdV) first provided an analytical description of solitons [8], which can be observed as either waves of elevation [9] or depression [10] on the surface of a fluid. Although KdV solitons have mainly been investigated experimentally in rectilinear geometries [9–13], examples in both curved and periodic media remain elusive.

A stable torus of fluid is a good experimental system to study solitons in a curved and periodic geometry. We manage to create such a stable torus of liquid by means of an original technique. We have previously studied linear waves propagating along the inner and outer torus borders [14]. Here, using this technique, we experimentally discover unreported periodic KdV solitons along a stable torus of liquid whose properties are fully characterized (profile, velocity, collision, and dissipation), and described with an experimentally validated model taking into account both the curved and periodic conditions. Our work thus paves the way to observe other nonlinear phenomena such as wave turbulence [15, 16], and soliton gas [17–21] in this specific geometry. Note that KdV solitons can be reached experimentally in curved geometries without periodicity (e.g., along the border of a liquid cylinder [22–24]), whereas trials have been attempted for periodic conditions in plane geometry (e.g., in an annular water tank [25, 26]), as well as for a curved and periodic system but only in a nonstationary regime and by applying a strong constraint to the liquid ring [27–29].

Theoretical works on solitons have yielded advanced mathematical techniques to study solutions to various integrable nonlinear equations [e.g., KdV, Nonlinear Schrödinger (NLS), Kadomtsev–Petviashvili], in particular the inverse scattering transform (IST) [30–33]. This nonlinear spectral analysis has been applied to experimental NLS solitons [21, 33], but remain scarce for KdV

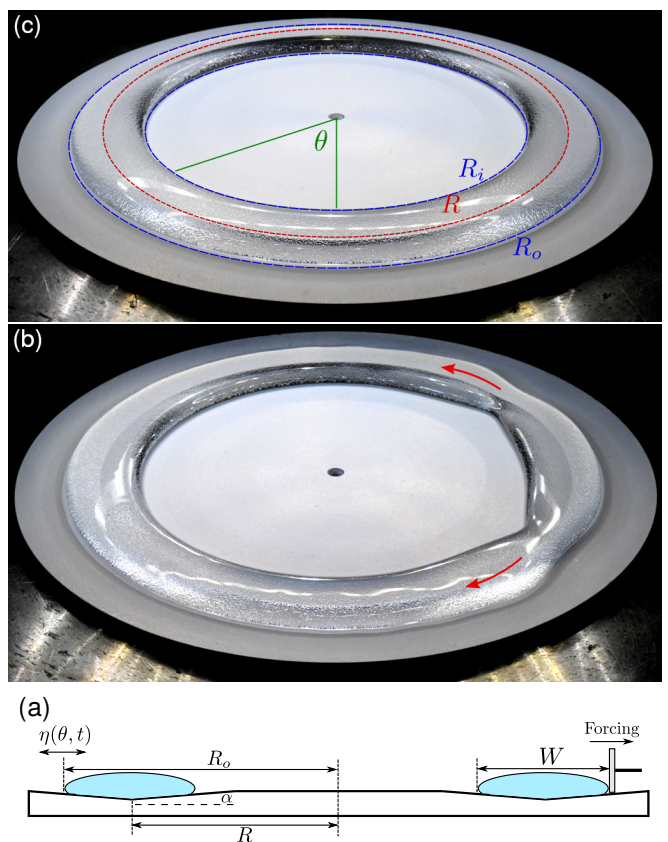


FIG. 1. (a) Schematic profile of the experimental setup. (b) Solitons propagating along the torus borders. (c) Stable liquid torus on a plate ($R_o = 7.9$ cm, $R = 7$ cm, $W = 1.8$ cm).

ones [34–36], and, so far, have not been applied to a periodic experimental system, a more complex setting which has recently received numerical and theoretical attention [33, 37–39].

Experimental setup.— We manage to create a stable torus of fluid by depositing distilled water on a superhydrophobic duralumin plate machined with a slightly slop-

ing triangular groove along the perimeter (see Fig. 1a-c) [14]. The radius of the groove center, R , is either 4 cm or 7 cm using two different substrates. The small angle α of the groove to the horizontal is 4.5° . We use a commercial superhydrophobic coating yielding a contact angle of 160° – 170° between liquid and substrate [14, 40] allowing the liquid torus to move with almost no constraint. To generate waves, the torus is impulse pulled (or pushed) horizontally using a linear actuator with a teflon plate attached to its end (see Fig. 1a). By deforming the meniscus, the actuator creates two counter-propagating solitons along the outer, and two along the inner, border of the torus (see Fig. 1b and movies in Supp. Mat. [41]). A camera located above the torus records the interface displacement. Using a border detection algorithm [42], we extract the azimuthal displacement $\eta(\theta, t)$, in the horizontal plane, of both the inner and outer torus borders. Measurements are made for various pulse amplitudes A and for different torus widths, W , by adding water. We set $\chi = R_o/R$, with R_o the outer radius of the torus, and $R_o = R + W/2$ (see Fig. 1a). χ thus quantifies the system curvature.

Soliton solutions.— When weak dispersion is balanced by weak nonlinearity, azimuthal waves $\eta(\theta, t)$ along a torus of fluid is governed at the leading order by a KdV equation with *periodic boundary conditions* as

$$\eta_t + \Omega_0 \left[\eta_\theta + \frac{5\chi^2}{4\widetilde{W}} \eta \eta_\theta + \frac{\chi^2 \widetilde{W}^2}{2R^2} \delta_{\text{Bo}} \eta_{\theta\theta\theta} \right] = 0, \quad (1)$$

with $\widetilde{W} = W/2$, $\delta_{\text{Bo}} = \text{Bo}_c - \text{Bo}$, and $\Omega_0 = (g_{\text{eff}} \widetilde{W})^{1/2}/R$ the angular phase velocity of linear gravity waves. The Bond number reads $\text{Bo} = \ell_{\text{eff}}^2 / (\widetilde{W}^2 \chi^4)$, its critical value $\text{Bo}_c \approx 1/6$, where $\ell_{\text{eff}} \equiv \sqrt{\sigma_{\text{eff}} / (\rho g_{\text{eff}})}$ is the effective capillary length, $\rho = 10^3 \text{ kg m}^{-3}$ is the fluid density, $g_{\text{eff}} = g \sin \alpha$ is the effective gravity, $g = 9.81 \text{ m s}^{-2}$, $\sigma_{\text{eff}} \simeq 60 \text{ mN m}^{-1}$ is an effective surface tension inferred by fitting the data; g_{eff} and σ_{eff} are, in particular, linked to the substrate geometry. We obtain Eq. (1) by using the dispersion relation of gravity-capillary waves along a liquid torus [14], and the periodic KdV equation formalism [24] (see Supp. Mat [41]).

Cnoidal wave solutions to Eq. (1) read

$$\eta(\theta, t) = A \text{cn}^2 \left(\frac{\theta - \Omega t}{\Delta \sqrt{m}} \middle| m \right) \text{ with } \Delta^2 = \frac{24}{5} \frac{\widetilde{W}^3}{AR^2} \delta_{\text{Bo}}, \quad (2)$$

where A is the (signed) amplitude and Δ the (angular) width of the solitary wave. Its velocity reads

$$\Omega = \Omega_0 \left[1 + \frac{5A}{6\widetilde{W}m} \chi^2 \left(1 - \frac{m}{2} - \frac{3E(m)}{2K(m)} \right) \right], \quad (3)$$

with $K(m)$ [resp. $E(m)$] the complete elliptic integral of the first (resp. second) kind. $m \in [0, 1]$ is the elliptic parameter for which the cnoidal function $\text{cn}(\theta|m)$

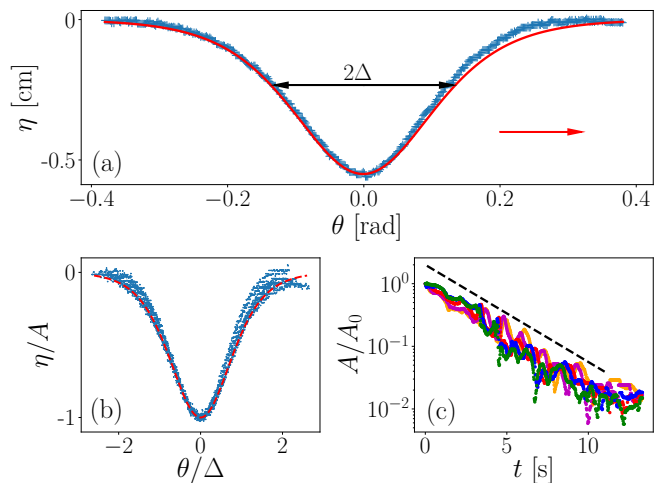


FIG. 2. a) (+) Experimental soliton profile at a fixed time. (–) Theoretical profile of Eq. (2) with no fitting parameter. b) Superimposition of rescaled soliton profiles during its propagation along one torus perimeter. (–) Eq. (2). c) Exponential damping of the soliton for different $W \in [2.2, 3]$ cm (2 mm step). $R = 7$ cm. Dashed line of slope $\tau = 2.8$ s.

is $\cos(\theta)$ for $m = 0$, and $\text{sech}(\theta)$ for $m = 1$ [13, 43]. In order to ensure 2π -periodicity, $K(m)$ must satisfy $\pi/\Delta = 4K(m)$ making m a function of A , and thus Ω a nonlinear function of A (see Supp. Mat. [41]). The periodic elliptic solutions of Eq. (2) are close to sech^2 for large enough R (e.g., for $R = 7$ cm, $1 - m \simeq 10^{-12}$). In that case, Eqs. (2)-(3) reduce to the classical solitary wave profile $\eta(\theta, t) = A \text{sech}^2[(\theta - \Omega t)/\Delta]$ and velocity $\Omega = \Omega_0 [1 + 5A\chi^2/(12\widetilde{W})]$. However, for smaller R (e.g. 4 cm), this classical solution cannot be used since the effect of periodicity, through Eq. (2)-(3), has to be taken into account (see below). Note that the experimental parameters used here are in the range of validity required for the derivation of Eq. (1) assuming weak dispersion $\mu = \widetilde{W}^2 \chi^2 \delta_{\text{Bo}} / (\Delta^2 R^2) \ll 1$ (i.e., shallow-water limit), weak nonlinearity $\epsilon = A\chi^2/\widetilde{W} \ll 1$, both of the same order of magnitude $\mu/\epsilon = \widetilde{W}^3 / (\Delta^2 R^2 A) \in [1, 3]$.

Soliton profile.— The pulse profile, $\eta(\theta, t)$, is extracted from the outer torus border (e.g., from the depression in Fig. 1b). Figure 2a shows that the experimental profile is well described by the theoretical soliton profile of Eq. (2) with no fitting parameter. Since a soliton balances theoretically dispersion and nonlinearity, it should also have a self-similar profile during its propagation. Figure 2b shows the superimposed rescaled profiles of a soliton during its propagation along almost one torus perimeter. The soliton (with this appropriate rescaling) thus conserves a self-similar shape during its propagation that is well described by Eq. (2), even if its amplitude decreases due to unavoidable dissipation. To quantify the latter, we plot in Fig. 2c the soliton amplitude as a function of time, $A(t)$, during two rounds

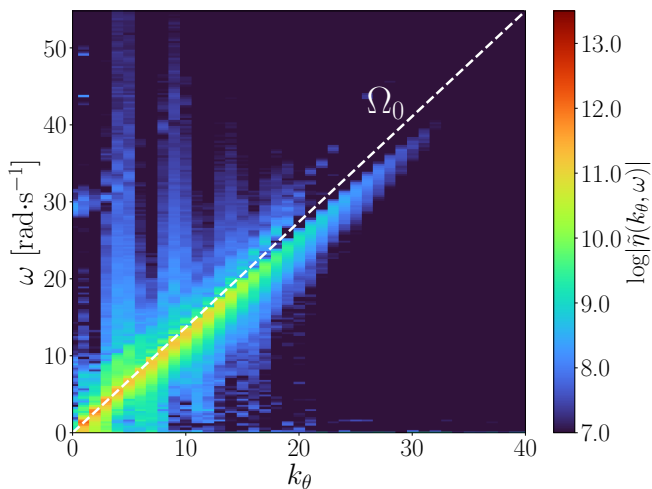


FIG. 3. Space-time Fourier spectrum $\tilde{\eta}(k_\theta, \omega)$ of the signal $\eta(\theta, t)$ (outer border). Dashed line: velocity $\Omega_0 = 1.37$ rad/s of long linear waves. The energy is concentrated around a linear branch of slope $\Omega < \Omega_0$, signature of a subsonic soliton.

along the torus. $A(t)/A(0)$ is found to decrease exponentially as $A(t) = A(0) \exp[-t/\tau]$, with a damping time τ found to be independent of the viscosity of the fluid used ($\nu \in [10^{-7}, 10^{-6}]$ m²/s, i.e., mercury or water), suggesting that dissipation probably comes from the triple contact line and not from the viscous dissipation.

Fourier spectrum.— We now compute the space-and-time Fourier transform, $\tilde{\eta}(k_\theta, \omega)$, of the signal $\eta(\theta, t)$ as shown in Fig. 3. The energy is found to be concentrated around a line of slope $\Omega = \omega/k_\theta$ corresponding to the pulse velocity. This quasi-nondispersive feature is a spectral signature of a soliton. The soliton velocity, Ω , is found to be slightly slower than long linear waves propagating at velocity Ω_0 (see Fig. 3), meaning the presence of a subsonic soliton. Note that a broadening of the soliton branch occurs due to nonlinearities, whereas low-intensity vertical traces (at low k_θ) correspond to mechanical noise.

Soliton width and velocity.— We now measure the typical soliton width Δ by fitting Eq. (2) to the experimental profile (as in Fig. 2a). Δ^2 is plotted in Fig. 4 for different pulse amplitudes, A , and torus widths W . Δ is found to scale as $\sqrt{W^3/A}$ in good agreement with Eq. (2)b with no fitting parameter (see solid line). We also measure the soliton velocity by time of flight during its propagation. The dimensionless pulse velocity, Ω/Ω_0 (i.e., Froude number), is displayed in the inset of Fig. 4 for various A and W . For large tori (i.e., using the substrate $R = 7$ cm for various W), the soliton velocity of Eq. (3) reduces to the classical KdV linear relationship, $\Omega/\Omega_0 = 1 + 5A\chi^2/(12\tilde{W})$ (see solid line), which is well verified experimentally (open circles). Depression solitons ($A < 0$) moving slower than linear waves ($\Omega/\Omega_0 < 1$ or subsonic) are

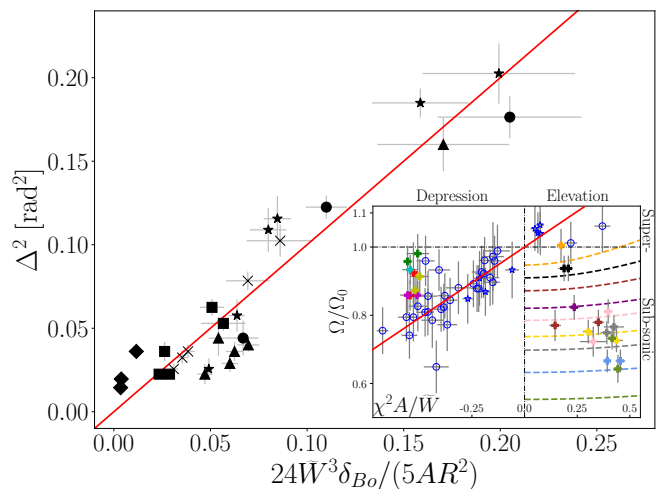


FIG. 4. Experimental soliton width squared Δ^2 for different amplitudes A and different widths $W \in [1.9, 4]$ cm (2 mm step). $R = 7$ cm. Solid line: Eq. (2) with no fitting parameter (slope 1). Inset: Dimensionless soliton velocity Ω/Ω_0 versus $A\chi^2/W$ for various A and W for $R = (+)$ 4 and (\circ) 7 cm. Dashed lines: Eq. (3) for different $W \in [2.8, 3.9]$. Solid line: classical KdV solution (slope 5/12). Occurrence of subsonic elevation solitons is due to effects of the periodic geometry.

observed for $\text{Bo} > \text{Bo}_c$, whereas elevation solitons ($A > 0$) are supersonic ($\Omega/\Omega_0 > 1$) for $0 \leq \text{Bo} < \text{Bo}_c$, as predicted for KdV in straight geometry [8, 10]. For smaller tori (i.e., $R = 4$ cm substrate), the relationship of Eq. (3) between velocity and amplitude is no longer linear (see dashed lines, and also Supp. Mat. [41]). In particular, we clearly observe *subsonic elevation* solitons due to the effects of the periodic geometry (see $+$ in the bottom right quadrant). The transition from subsonic to supersonic solitons occurs, from Eq. (3), at $m^* = 2 - 3E(m^*)/K(m^*) \simeq 0.96$ regardless of Bo . We sum up the solutions of periodic KdV equation as

$$\begin{aligned} \text{Bo} < \text{Bo}_c: \text{Elevation, } & \underbrace{0}_{\text{subsonic}} \quad \underbrace{m^*}_{\text{supersonic}} \quad \underbrace{1}_{\text{supersonic}} \quad \underbrace{m}_{\text{supersonic}} \\ \text{Bo} > \text{Bo}_c: \text{Depression, } & \underbrace{0}_{\text{subsonic}} \quad \underbrace{m^*}_{\text{subsonic}} \quad \underbrace{1}_{\text{subsonic}} \quad \underbrace{m}_{\text{subsonic}} \end{aligned}$$

Note that certain types of solitons are unreachable here within our finite ranges of \tilde{W} and of A .

Critical Bond number.— The critical Bond number corresponds to transition between elevation and depression soliton solutions [10]. It is remarkable that our theoretical value of the critical Bond number $\text{Bo}_c \approx 1/6$ for a torus differs from the value $1/3$ for the plane geometry case [8]. Indeed, Bo_c strongly depends on the slope α as found numerically [24]. Equating the Bond expression to $1/6$ and inserting $\tilde{W} = R_o - R$, we find the critical outer radius R_o^c of the torus separating elevation and depression solitons as $R_o^c{}^3 - R_o^c{}^2 R - \sqrt{6}\ell_{\text{eff}} R^2 = 0$, and thus $R_o^c = 8.43$ cm for our parameters. Experimentally, we have a range of $\text{Bo} \in [0.09, 0.5]$ by varying R_o , and we

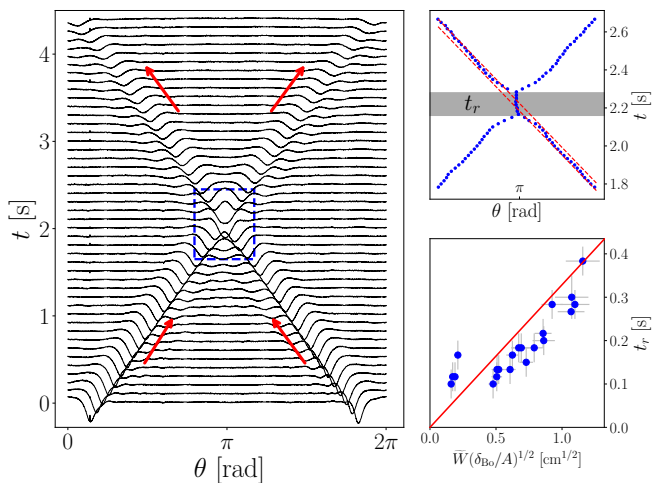


FIG. 5. Angle-time plot of a head-on collision between two depression solitons propagating along a torus. Top: Enlargement (dashed square) showing the soliton minima, phase shift, and residence time t_r . Bottom: t_r vs $\widetilde{W}\sqrt{\delta_{B_0}/A}$ for various A and W . Solid line slope is $0.33\text{ s/m}^{1/2}$. $R_o = 8.2\text{ cm}$.

look for the occurrence of the transition from depression ($R_o < R_o^c$) to elevation ($R_o > R_o^c$) solitons by increasing R_o . For small R_o , depression solitons are indeed observed, whereas elevation solitons are detected above a certain radius. We find a critical experimental radius of $R_o^c = 8.4 \pm 0.02\text{ cm}$ in good agreement with the above predictions. This corresponds to $\text{Bo}_c = 0.17$ close to the theoretical value $1/6$. This result is also confirmed when using the other substrate ($R = 4\text{ cm}$).

Soliton collision.— The nonlinear nature of the solitons is further confirmed by observing the collisions of two depression solitary waves as illustrated in Fig. 5. The top inset shows an enlargement of the two solitary wave minima as they collide. The collision evidences a long residence time t_r (of the order of 0.1 s) during collision, and a slight phase shift, a feature of solitons. Inset of Fig. (5) shows that t_r is experimentally found to scale as $t_r \sim \widetilde{W}\sqrt{\delta_{B_0}/A}$, matching our prediction (see Supp. Mat. [41]) and extending the pure gravity prediction [44].

Direct scattering.— We have shown above that solitons observed along a liquid torus are well described by Eqs. (2)-(3), solutions of the periodic KdV Eq. (1). We now implement a nonlinear spectral analysis, using the periodic inverse scattering transform (PIST), to find the discrete eigenvalue λ of each soliton in our signals [32]. Note that such a method has not been applied so far to an experimental periodic system with a significant discreteness in Fourier space. We associate with Eq. (1) the following eigenvalue problem [32, 37]

$$\psi_{xx} + [\beta\eta(x, t = t_0) + \lambda]\psi = 0, \quad (4)$$

subjected to periodic boundary conditions, with period $L = 2\pi R_o$, and $\beta = 5/(12\widetilde{W}^3\chi^2\delta_{B_0})$. The eigenval-

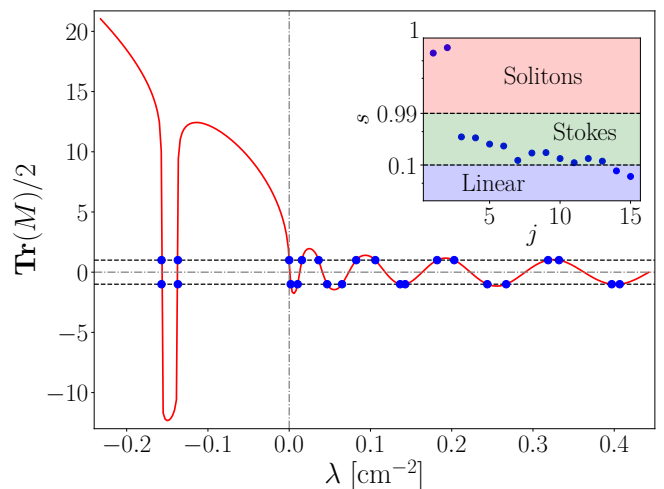


FIG. 6. PIST detection of solitons. $\text{Tr}[M(\lambda)]/2$ (red line) for the signal of Fig. 5 at $t_0 = 2.7\text{ s}$, with the associated nonlinear spectrum (bullets). Two solitons are detected (bullets for $\lambda < 0$). Inset: Soliton index s for different azimuthal wave numbers j revealing two solitons ($s > 0.99$). Lin-Logit scale.

ues correspond to either bounded solutions, i.e., solitons, for $\lambda < 0$, and Stokes waves or radiative phonons for $\lambda \geq 0$ [31]. We use a periodic scattering matrix $M(\lambda)$ (called monodromy matrix) to translate the solutions of Eq. (4) by one period. The nonlinear spectrum is then given by the condition $\text{Tr}[M(\lambda)]/2 = \pm 1$. The experimental nonlinear spectrum is displayed in Fig. 6 (bullets), along with the half-trace of the matrix M (solid line) for the signal in Fig. 5 at a time t_0 . Two solitons are detected in Fig. 6 for which $\text{Tr}[M(\lambda)]/2 = \pm 1$ (4 eigenvalues), corresponding to two distinct values $\lambda < 0$. From this nonlinear spectrum, we compute the soliton index s for each nonlinear mode as $s = \frac{\lambda_{2j+1} - \lambda_{2j}}{\lambda_{2j+1} - \lambda_{2j-1}}$ [34] which corresponds to solitons if $s > 0.99$, Stokes waves if $s > 0.5$, or linear radiative modes if $s < 0.5$ [45]. We are thus able to count the number of solitons included in a given signal, e.g., the one in Fig. 5. Indeed, the inset of Fig. 6 confirms the presence of 2 solitons, as expected. Beyond the validity of PIST to detect KdV solitons in a periodic system, PIST could be also be applied to directly generate a KdV soliton gas in such geometry.

Conclusion.— We demonstrated the existence of solitons in a system with periodic and curved boundary conditions. They are observed propagating along a stable torus of fluid (created by a technique we developed) and are fully characterized (profile, velocity, collision, dissipation and nondispersive features). These unexplored solitons are found to be governed by a KdV equation with *periodic boundary conditions* leading to significant differences with infinite straight-line KdV solitons, such as the observation of subsonic elevation solitons, and the prediction of a nonlinear dependence of the soliton velocity on its amplitude. A nonlinear spectral analysis of solitons is

implemented (PIST) and is experimentally validated for the first time for periodic conditions. Our work is not restricted to hydrodynamics, and thus could be applied to other domains involving periodic systems governed by a KdV equation. Quantifying the role of dissipation breaking integrability is also of primary interest [46]. In the future, this new system could address the possible existence of KdV soliton gas [17–21] in periodic systems, and their collision [47], as well as of Kaup-Boussinesq bidirectional solitons [20, 48, 49] with corresponding finite-gap spectral methods [50].

We thank A. Di Palma and Y. Le Goas for technical help on the experimental setup. Part of this work was supported by the French National Research Agency (ANR SoGood project No. ANR-21-CE30-0061-04), and by a grant from the Simons Foundation MPS N°651463.

* E-mail: filip.novkoski@u-paris.fr

† E-mail: chi-tuong.pham@upsaclay.fr

‡ E-mail: eric.falcon@u-paris.fr

- [1] J. S. Russell, Proc. R. Soc. Edinburgh **11**, 319 (1844).
- [2] H.-Y. Hao and H. J. Maris, Phys. Rev. B **64**, 064302 (2001).
- [3] N. J. Zabusky and M. D. Kruskal, Phys. Rev. Lett. **15**, 240 (1965).
- [4] T. Yu. Astakhova, M. Menon, and G. A. Vinogradov, Phys. Rev. B **70** 125409 (2004).
- [5] L. Pitaevskii and S. Stringari, *Bose-Einstein Condensation* (Oxford University Press, Oxford, 2003).
- [6] G. A. El, A. Gammal, and A. M. Kamchatnov, Phys. Rev. Lett. **97**, 180405 (2006).
- [7] S. Yomosa, J. Phys. Soc. Jpn **56**, 506 (1987).
- [8] D. J. Korteweg and G. de Vries, London, Edinburgh, Dublin Philos. Mag. J Sci. **39**, 422 (1895).
- [9] J. L. Hammack and H. Segur, J. Fluid Mech. **65**, 289 (1974).
- [10] E. Falcon, C. Laroche, and S. Fauve, Phys. Rev. Lett. **89** 204501 (2002).
- [11] M. Remoissenet, *Waves Called Solitons* (Springer-Verlag, Heidelberg, 3rd ed., 1999).
- [12] T. Dauxois and M. Peyrard, *Physics of Solitons* (Cambridge University Press, Cambridge, 2006).
- [13] R. H. J. Grimshaw, *Solitary Waves in Fluids* (WITPress, Southampton, 2007).
- [14] F. Novkoski, E. Falcon, and C.-T. Pham, Phys. Rev. Lett. **127**, 144504 (2021).
- [15] E. Falcon and N. Mordant, Annu. Rev. Fluid Mech. **54**, 1 (2022).
- [16] G. Ricard and E. Falcon, EPL (Europhys. Lett.) **135**, 64001 (2021).
- [17] V. E. Zakharov, Sov. Phys. JETP **33**, 538 (1971).
- [18] G. A. El and A. M. Kamchatnov, Phys. Rev. Lett. **95**, 204101 (2005).
- [19] A. Costa, A. R. Osborne, D. T. Resio, S. Alessio, E. Crivì, E. Saggese, K. Bellomo, and C. E. Long, Phys. Rev. Lett. **113**, 108501 (2014).
- [20] I. Redor, E. Barthélemy, H. Michallet, M. Onorato, and N. Mordant, Phys. Rev. Lett. **122**, 214502 (2019).
- [21] P. Suret, A. Tikan, F. Bonnefoy, F. Copie, G. Ducrozet, A. Gelash, G. Prabhudesai, G. Michel, A. Cazaubiel, E. Falcon, G. El, and S. Randoux, Phys. Rev. Lett. **125**, 264101 (2020).
- [22] E. Bourdin, J.-C. Bacri, and E. Falcon, Phys. Rev. Lett. **104**, 094502 (2010).
- [23] S. Perrard, L. Deike, C. Duchêne, and C.-T. Pham, Phys. Rev. E **92**, 011002(R) (2015).
- [24] G. Le Doudic, S. Perrard, and C.-T. Pham, J. Fluid Mech. **923** A13 (2021).
- [25] A. Shi, M. H. Teng, and T. Y. Wu, J. Fluid Mech. **362**, 157 (1998).
- [26] T. G. Elizarova, M. A. Istomina, and N. K. Shelkovnikov, Math. Models Comput. Simul. **4**, 552 (2012).
- [27] S. Perrard, Y. Couder, E. Fort, and L. Limat, EPL (Europhys. Lett.) **100**, 54006 (2012).
- [28] A. Ludu and A. Raghavendra, Appl. Numer. Math. **141**, 167 (2019).
- [29] H. Ait Abderrahmane, P. S. Sedeh, H. D. Ng, and G. H. Vatistas, Phys. Rev. E **99**, 023110 (2019).
- [30] C. S. Gardner, J. M. Greene, M. D. Kruskal, and R. M. Miura, Phys. Rev. Lett. **19**, 1095 (1967).
- [31] M. J. Ablowitz and H. Segur, *Solitons and the Inverse Scattering Transform* (Society for Industrial and Applied Mathematics, Philadelphia, 1981).
- [32] P. G. Drazin and R. S. Johnson, *Solitons: An Introduction* (Cambridge University Press, 1989).
- [33] A. R. Osborne, *Nonlinear Ocean Waves and the Inverse Scattering Transform* (Academic Press, London, 2010).
- [34] I. Christov, Math. Comput. Simulat. **80**, 192 (2009).
- [35] A. R. Osborne and T. L. Burch, Science **208**, 451 (1980).
- [36] I. Redor, H. Michallet, N. Mordant, and E. Barthélemy, Phys. Rev. Fluids **6**, 124801 (2021).
- [37] A. R. Osborne and L. Bergamasco, Physica D-Nonlinear Phenomena **18**, 26 (1986).
- [38] A. R. Osborne, Math. Comput. Simulat. **37**, 431 (1994).
- [39] Ivan C. Christov, Math. Comput. Simulat. **82**, 1069 (2012).
- [40] R. Gupta, V. Vaikuntanathan, and D. Sivakumar, Colloid. Surface A **500**, 45 (2016).
- [41] See Supplemental Material at <http://link.aps.org/>... for movies and further data analyses.
- [42] Filip Novkoski, Circular border detection in Python, <https://github.com/nofko/PYtorus> (2020).
- [43] M. Abramowitz and I. A. Stegun, *Handbook of mathematical functions with formulas, graphs, and mathematical tables, Vol. 55* (US Government printing office, 1964).
- [44] H. Power and A. T. Chwang, Wave Motion **6**, 183 (1984).
- [45] A. R. Osborne, Phys. Rev. E **52**, 1105 (1995).
- [46] I. S. Chekhovskoy, O. V. Shtyrina, M. P. Fedoruk, S. B. Medvedev, and S. K. Turitsyn, Phys. Rev. Lett. **122**, 153901 (2019).
- [47] F. Carbone, D. Dutykh, and G. A. El, EPL (Europhysics Letters) **113**, 30003 (2016).
- [48] J. E. Zhang and Y. Li, Phys. Rev. E **67**, 016306 (2003).
- [49] T. Congy, G. El, and G. Roberti, Phys. Rev. E **103**, 042201 (2021).
- [50] A. O. Smirnov, Theor. Math. Phys. **66**, 19 (1986).

Supplemental Materials

“Experimental Periodic Korteweg-de Vries Solitons along a Torus of Fluid”

Filip Novkoski,¹ Chi-Tuong Pham,² and Eric Falcon¹

¹*Université Paris Cité, MSC, UMR 7057 CNRS, F-75013 Paris, France*

²*Université Paris-Saclay, LISN, UMR 9015 CNRS, F-91405 Orsay, France*

(Dated: March 22, 2022)

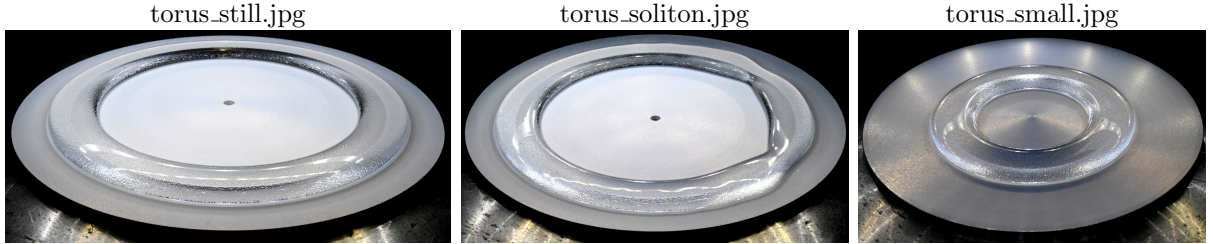
In this supplemental material, we present movies (Sec. I) and images (Sec. II) of solitons propagating on a torus of fluid. Details on the elliptic solutions of the Korteweg-de Vries (KdV) equation with periodic boundary conditions are discussed, including effects on soliton velocity (Sec. III), which is followed by a discussion on the form of the KdV equation for a torus (Sec. IV). The residence time of a soliton during collision is also detailed (Sec. V). Methods used to obtain the nonlinear spectral analysis are described (Sec. VI).

I. MOVIES

- soliton_large.mp4 (10 s): Two depression solitons along a torus of width 2.7 cm. $R = 7$ cm substrate.
- soliton_small_depression.mp4 (10 s): Two depression solitons along a torus of width 2.5 cm. $R = 4$ cm substrate.
- soliton_small_elevation.mp4 (12 s): Two elevation solitons along a torus of width 3.4 cm. $R = 4$ cm substrate.

II. IMAGES

- torus_still.png: View of a still torus of liquid on a substrate (groove at $R = 7$ cm).
- torus_soliton.jpg: Two solitons propagating on each border of the torus. Same substrate (groove at $R = 7$ cm).
- torus_small.jpg: View of still torus of liquid on another substrate (groove at $R = 4$ cm).



III. PERIODIC SOLUTIONS OF KDV EQUATION

The condition of periodicity of the cnoidal function, solution of Eq. (2) of the main text, yields

$$\frac{2\pi}{N_\theta \Delta} = 4K(m), \text{ i.e., } 2\pi = 8N_\theta \sqrt{\frac{6\widetilde{W}^3 m \delta_{Bo}}{5R^2 A}} K(m), \quad (\text{S1})$$

where N_θ is the number of solitons and $K(m)$ is the complete elliptic integral of the first kind.

As shown in Fig. S1a (for different soliton widths W), this periodicity condition links the amplitude, A , and the elliptic parameter, $m \in [0, 1]$, in a bijective manner. Experimentally, we cannot reach values of $|A|/W$ larger than 0.2 due to stability reasons of the torus. As a consequence, Fig. S1a shows that supersonic elevation solitons with cnoidal profiles (occurring only for $m^* < m < 1$) cannot be observable within our ranges of torus width and soliton amplitude.

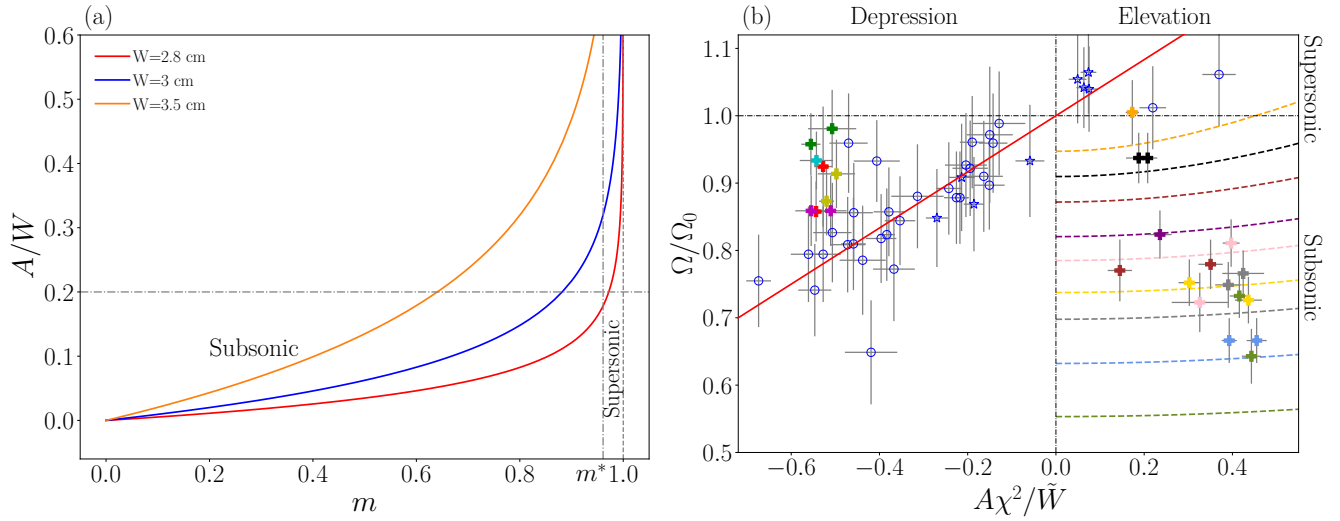


FIG. S1. (a) Amplitude A of elevation soliton in units of the torus width W versus the elliptic parameter m as given by the periodicity condition of Eq. (S1) for three different widths. $N_\theta = 2$. $m^* = 0.96$ corresponds to the transition between subsonic and supersonic elevation solitons. $Bo > Bo_c$. $R = 4$ cm. (b) Inset of Fig. 4 of the main text.

As stressed in the main text, the cnoidal function $\text{cn}(\theta|m)$ of Eq. (2) reduces to $\cos(\theta)$ for $m = 0$, and $\text{sech}(\theta)$ for $m = 1$. Inserting $m = 0.999$ into the periodicity condition of Eq. (S1) for a fixed soliton amplitude, we find the phase diagram in the (R, W) parameter space showing the transition between cnoidal soliton profiles (green regions) and quasi-sech soliton profiles (orange region). For tori with a small radius (e.g., $R = 4$ cm), one indeed reports the observation of solitons with either a cnoidal profile or a sech one. Conversely, for tori with a $R = 7$ cm radius (larger substrate), only sech solitons can be observed as found experimentally.

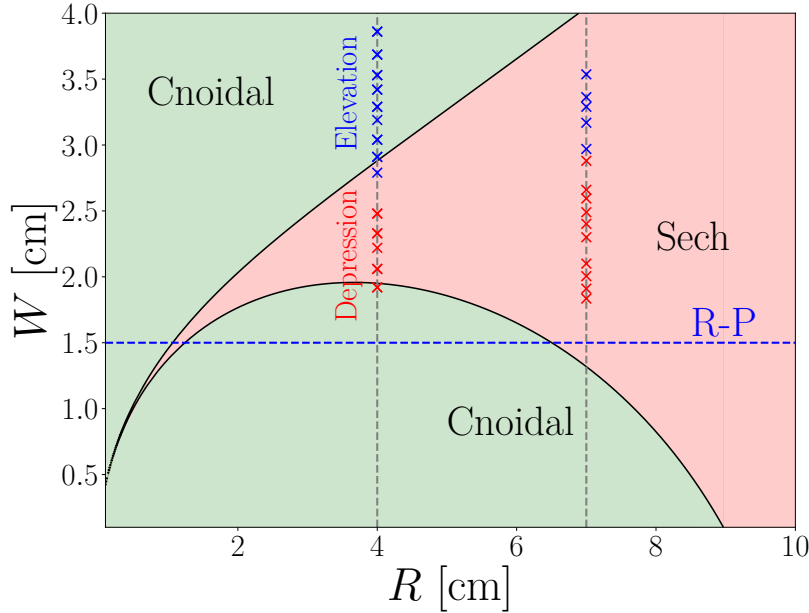


FIG. S2. Phase diagram in the (R, W) parameter space showing the transition between theoretical cnoidal soliton profiles (green regions) and quasi-sech soliton profiles (orange region) as given by the periodicity condition of Eq. (S1) for a chosen soliton amplitude ($A/W = 0.2$) and elliptic parameter $m = 0.999$. $N_\theta = 2$. The experimental range of torus widths is typically $W \in [1.5, 4]$ cm. Experimentally studied torus widths (\times -symbols) for two different torus radii $R = 4$ cm and $R = 7$ cm (vertical dashed lines). R-P denotes the Rayleigh-Plateau instability occurring for a thin enough torus.

IV. KDV EQUATION FOR A TORUS

Using the same notation as in the main text, the dispersion relation of gravity-capillary waves along a torus of fluid reads

$$\omega^2 = \left(g_{\text{eff}} \frac{k_\theta}{R_o} + \frac{\sigma_{\text{eff}}}{\rho} \frac{k_\theta^3}{R_o^3} \right) \phi \left(\frac{k_\theta}{R_o} \chi^2 \widetilde{W} \right). \quad (\text{S2})$$

with $\phi(x) \approx \tanh(x)$ [24]. Expanding for $k_\theta \rightarrow 0$, using $\phi(x) \approx x - x^3 \phi'''(0)/6$, Eq. (S2) reads

$$\omega^2 = \Omega_0^2 k_\theta^2 \left[1 + \frac{k_\theta^2}{R_o^2} \widetilde{W}^2 \chi^2 (\text{Bo} - \text{Bo}_c) \right], \quad (\text{S3})$$

with $\text{Bo}_c = \phi'''(0)/6 \approx 1/6$. By taking the root of Eq. (S3) we find

$$\omega \approx \Omega_0 k_\theta \left[1 + \frac{k_\theta^2}{2R_o^2} \widetilde{W}^2 \chi^2 (\text{Bo} - \text{Bo}_c) \right]. \quad (\text{S4})$$

Replacing ω and k_θ by $i\partial_t$ and $-i\partial_\theta$ respectively, we recover the linear terms of the KdV Eq. (1). We introduce the nonlinear term by normalizing it with \widetilde{W} as in [24]. Since with each k_θ there is an associated factor of χ^2 for the dispersive terms, we include it with the nonlinear term as well. The numerical factor of 5/4 comes from the groove shape of the substrate, as numerically and experimentally verified in a straight geometry [24].

V. RESIDENCE TIME OF COLLISION

For pure gravity waves, i.e., $\text{Bo} \ll \text{Bo}_c$, the residence time during a head-on collision between two KdV solitons in a straight geometry is approximately given to first order by [44]

$$t_r = \ln \left(\frac{\sqrt{3} + 1}{\sqrt{3} - 1} \right) \frac{2\mu}{k\sqrt{3}gh\epsilon}, \quad (\text{S5})$$

where μ is the dispersion parameter, ϵ is the nonlinearity one, h is the water depth and k is the typical wavenumber. Simply applying this result to our gravity-capillary KdV Eq. (1) yields

$$t_r = 2\sqrt{\frac{6}{5}} \ln \left(\frac{\sqrt{3} + 1}{\sqrt{3} - 1} \right) \frac{\widetilde{W}}{\sqrt{g_{\text{eff}} A}} \sqrt{\delta_{\text{Bo}}} \simeq 0.33[\text{s/m}^{1/2}] \widetilde{W} \sqrt{\frac{\delta_{\text{Bo}}}{A}}. \quad (\text{S6})$$

VI. NUMERICAL METHODS FOR NONLINEAR SPECTRAL ANALYSIS

We largely follow [35,38] in order to obtain the PIST detection of solitons within our experimental signal. As mentioned before, we are looking, at fixed time $t = t_0$, for eigenvalues of the associated Schrödinger problem

$$\psi_{xx} + [\beta\eta(x, t = t_0) + \lambda] \psi = 0, \quad (\text{S7})$$

subjected to periodic boundary conditions, with period $L = 2R_o\pi$, and $\beta = 5/(12\widetilde{W}^3\chi^2\delta_{\text{Bo}})$. Floquet's theorem allows us to write for the fundamental solution matrix Φ as

$$\Phi(x + L; x_0, \lambda) = M(x_0, \lambda)\Phi(x; x_0, \lambda), \quad (\text{S8})$$

where we have introduced the monodromy matrix

$$M(x_0, \lambda) = \begin{pmatrix} a & b \\ b^* & a^* \end{pmatrix} (x_0, \lambda). \quad (\text{S9})$$

It follows that we obtain periodic or antiperiodic solutions when

$$|\mathbf{Tr}(M)| = 2. \quad (\text{S10})$$

In practice we consider a signal $\eta(x)$ consisting of N points on an interval discretized by Δx . Since we do not have direct access to the monodromy matrix, we are led to look at the following closely related scattering matrix

$$S = \prod_{i=N-1}^0 T \quad \text{where} \quad T = \begin{pmatrix} \cos(k\Delta x) & \sin(k\Delta x)/k \\ -k \sin(k\Delta x) & \cos(k\Delta x) \end{pmatrix} (x, \lambda), \quad (\text{S11})$$

where $k = \sqrt{\beta\eta(x) + \lambda}$. The monodromy matrix M and the above scattering matrix are related through

$$\mathbf{Tr}(M) = \mathbf{Tr}(S), \quad (\text{S12})$$

$$M_{21} = S_{12}. \quad (\text{S13})$$

For a given signal $\eta(x)$, with $N = 3801$, we calculate the matrix S and its trace for each value of λ in an interval $[\lambda_{\min}, \lambda_{\max}]$, where $\lambda_{\min} = -\beta[\max(\eta) - \langle \eta \rangle_x]$ and $\lambda_{\max} = \lambda_{\min} + 2|\lambda_{\min}|$, in order to obtain Fig. 6 of the main paper.

To obtain the soliton spectrum of Fig. 6, we look for zeros of $|\mathbf{Tr}(M)|/2 - 1$. This is done by first finding the maxima and minima for a set of $|\mathbf{Tr}(M)|/2$ calculated on N points in the given interval. We use the pairs of λ of those extrema as bounds for the bisection method, through which we then find the zeros to a tolerance of 10^{-12} . These methods should remain valid, despite the bidirectionality of the system, as long as solitons are locally KdV [48], that is far enough from interacting with each other.